Map of Sky background brightness temperature at L-band

E.P. Dinnat, D.M. Le Vine, S. Abraham and N. Floury

Abstract

This document describes a map for brightness temperature of the cold sky for use in remote sensing at L-band. The sky map consists of an effective brightness temperature comprised of three terms: Cosmic background, Hydrogen line emission, and continuum emission. The map is designed for use in the protected window at 1.413 GHz and is based on radio astronomy surveys in the window.

Contents

1 Introduction

1.1 Background summary

The spectral window at L-band (1.400-1.427 GHz) reserved for passive use only is important in microwave remote sensing for measuring parameters such as soil moisture and ocean salinity. At this frequency, radiation from celestial sources such as those in our galaxy can be significant and, unlike the constant cosmic background, spatially variable across the sky. A good description is needed for calibration (e.g. looking at cold sky) and to make corrections for the down-welling radiation that is reflected from the surface and detected by the sensor.

In addition to the cosmic background, the source of the radiation in the window at 1.4 GHz is line emission from neutral hydrogen and broadband (continuum) emission. Sources within our solar system such as the Sun and Moon are not included. Radio astronomy measurements in this window have been made with modern instruments. This data has been converted into an equivalent thermal source with brightness

$$B(\Omega, \nu) = 2kT_b(\Omega, \nu)/\lambda^2. \tag{1}$$

The equivalent brightness temperature $T_b(\Omega, \nu)$ in the equation above has the characteristic that if it is integrated over the passband of a radiometer with a bandwidth of $\Delta B_A = 26$MHz in the interval between $1.401 - 1.427$ GHz, one obtains the same result one would obtain by integrating the actual data from the radio astronomy surveys. The conversion to passbands of other widths is described in the text. The reason for choosing the passband above is that it is representative of the Aquarius radiometer which motivated these studies [1]. In deriving the equivalent brightness temperature, it is assumed that the radiation is unpolarized. Section 2 below describes in more detail how the equivalent brightness temperature was obtained from the radio astronomy measurements.

1.2 Final data format description and distribution

The data are presented as maps of the equivalent brightness temperature $T_b(\Omega, \nu)$ in celestial coordinates. The data file is distributed by the NASA Physical Oceanography Distributed Active Archive Center (PO.DAAC) at https://podaac.jpl.nasa.gov/dataset/AQUARIUS_ANCILLARY_CELESTIALSKY_V1 (or ftp://podaac-ftp.jpl.nasa.gov/allData/aquarius/L3/mapped/galaxy).

All maps contain $721 \times 1441 = 1038961$ values, which is the number of elements for a map for declination between $\delta = -90°$ and $\delta = +90°$ at $0.25°$ resolution and right ascension between $\alpha = 0°$ and $\alpha = 360°$ at $0.25°$ resolution.

2 Methodology: derivation of the equivalent brightness temperature map

The brightness temperature of the sky background T_{Sky} is derived from the sum of three components: The brightness temperature of the continuum T_{Cont} (including, as a separate term, the effective emission of Cassiopeia $T^*_{\text{Cas }A}$), the effective brightness temperature of the atomic hydrogen T^*_{HI} and the cosmic microwave background T_{CMB}

$$T_{\text{Sky}} = T_{\text{Cont}} + T^*_{\text{Cas }A} + T^*_{\text{HI}} + T_{\text{CMB}}. \tag{2}$$

The contribution from Cassiopeia A was excluded from the reference continuum survey, because of its strength and variability. We have added it back using another survey (see 2.3).

2.1 Continuum and Cosmic Microwave Background (CMB)

The brightness temperature of the continuum plus CMB was measured by Reich and Reich [2, 3] for the northern sky (declinations larger than $-20°$), and by Testori et al. and Reich et al. [4, 5] for the southern sky. The measurements were performed at central frequency $\nu_0 = 1420$ MHz with an effective bandwidth $\Delta B_C = 18$ MHz. The bandwidth spreaded over $B_C = \nu_0 \pm 10$ MHz

with an exclusion band of $\pm 1\,\text{MHz}$ centered on ν_0. The exclusion window is the location of the hydrogen line. The assumption is made that the continuum T_b is flat (independent of frequency) over the radiometer bandwidth. Hence the slight difference between the central frequencies of the sky survey and the radiometer (e.g. Aquarius radiometer) is neglected (see A and B), as well as the fact that T_{Cont} varies slightly over the band $B_{\mathcal{A}} = [1.401 - 1.427]\,\text{GHz}$ (see A and C).

The continuum data are shown in Fig. 1 in clestial coordinates (ECI) for the epoch J2000. The data for the southern hemisphere were provided as a personal communication. The northern sky data are available for download at `http://www.mpifr-bonn.mpg.de/survey.html`. The data consist of a map of 721x1441 values of T_b, corresponding to a resolution of $0.25°$ in both coordinates.
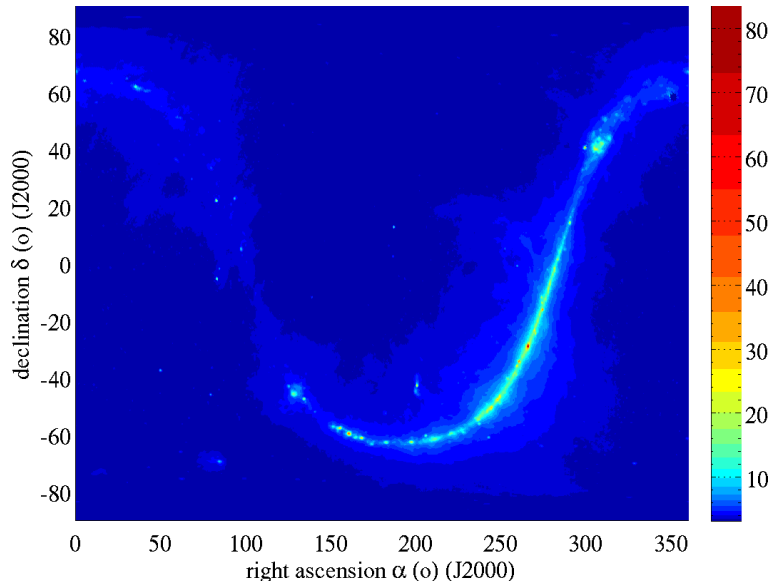

Figure 1: Sum of T_{Cont} and T_{CMB} (K) in equatorial coordinates in epoch J2000.

2.2   Atomic hydrogen HI

The HI line emission was measured by Hartmann and Burton [6] for the northern sky, and Arnal et al. [7] for the southern sky. Data were merged by Kalberla et al. [8] as a whole sky map, including a correction for stray radiation, at 891 different frequencies in the domain $\nu_0 \pm 2.17\,\text{MHz}$ (equivalently: the measurements span between ± 460 km/s Doppler velocities with a constant 1.03 km/s resolution). Contrary to the continuum, HI emission varies significantly with frequency even close to ν_0, so that its T_b is not constant over the band $B_{\mathcal{A}}$. Therefore, we define an effective brightness temperature T_{HI}^* derived from the integral (see D)

$$T_{\text{HI}}^* = \frac{1}{\Delta B_{\mathcal{A}}} \int_{\nu_0 - 1\,\text{MHz}}^{\nu_0 + 1\,\text{MHz}} T_{\text{HI}}(\nu)d\nu \qquad (3)$$

where $T_{\text{HI}}(\nu)$ is the T_b of HI at the frequency ν over the bandwidth $d\nu$, and is integrated over the band $B_{\text{HI}} = \nu_0 \pm 1\,\text{MHz}$ that was excluded in the continuum survey [1]. Because $B_{\mathcal{A}}$ overlaps B_{HI}, the total flux of HI in the 2 MHz bandwidth has to be conserved when measured by the radiometer. Therefore, the integral is normalized by the radiometer bandwidth, $\Delta B_{\mathcal{A}}$. One can verify that the flux emitted by HI in the band B_{HI} and the one measured by the instrument in the band $B_{\mathcal{A}}$ are the same.

Note: for another instrument measuring in the band B' (with bandwidth $\Delta B'$) overlapping B_{HI}, the map can be renormalized according to $T_{\text{HI}}^{*'} = (\Delta B_{\mathcal{A}} \,/\, \Delta B')T_{\text{HI}}^*$.

We use a sub-data set of 485 values limited to about $\pm$ 250 km/s Doppler shifts. The data are downloadable at `http://cdsarc.u-strasbg.fr/ftp/cats/VIII/76/lab250.fit.gz` The file

---

[1] The flux radiated by HI at frequencies beyond $\nu_0 \pm 1\,\text{MHz}$ is included in the continuum map.
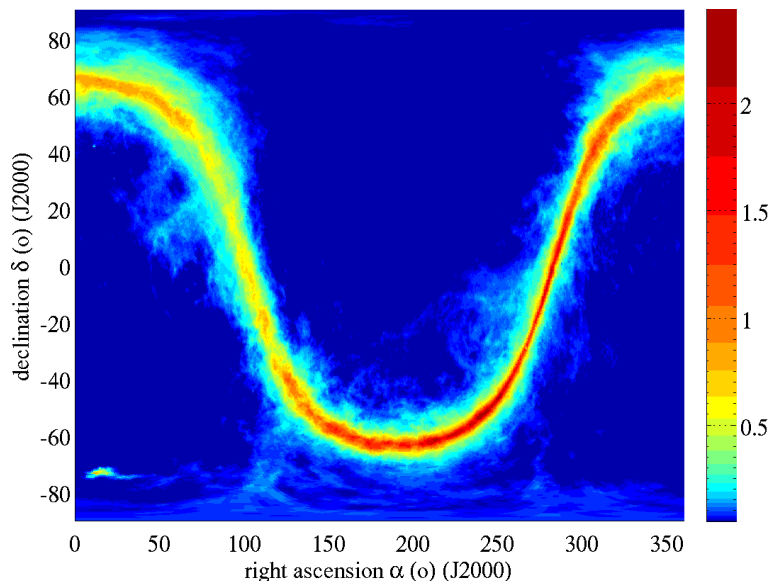
Figure 2: Effective brightness temperature of HI, T_{HI}^* (K), integrated over a 2 MHz bandwidth centered on ν_0 and normalized over a bandwidth $\Delta B_{\mathcal{A}} = 26$ MHz, in equatorial coordinates in epoch J2000.

contains a 3D map with a resolution of $0.5° \times 0.5°$ in galactic longitude and latitude, and about 1.03 km/s in velocity. The data are interpolated in the ECI J2000 reference frame at 0.25° resolution in declination and right ascension (nearest neighbor) after the integration over the spectral band in (3) is performed for the data in the galactic reference frame.

2.3 Cassiopeia A

Because of its large flux density, the supernova remnant Cassiopeia A could not be included in the continuum survey, resulting in a small portion of the Sky map having missing pixels around that source. The location[2] of Cassiopeia A is ($\alpha = 350.86°; \delta = 58.81°$) in epoch J2000 [10], its diameter is a few arcmins [9]. Its flux density varies with frequency and time. We use a flux density $S_{CasA} = 1600$ Jy at 1414 MHz for the period 2010-2013 (1 Jansky (Jy) is 10^{-26} W/m^2/Hz), as explained in E. Figure 3 reports the location of Cassiopeia A in the sky and the surrounding so-called missing pixels in the continuum survey.

An effective T_b is derived, assuming the T_b is homogeneous over a pixel in the map, according to

$$T_{Cas\,A} = \frac{\lambda^2}{2k} \frac{S_{CasA}}{\Omega_p},$$ (4)

with $\Omega_p = \cos\delta(0.25°)^2 \simeq 9.8572 \times 10^{-6}$ sr, the solid angle of a pixel of size $0.25° \times 0.25°$ at a declination δ. Fig. 4 reports the Cassiopeia A brightness temperature when it is arbitrarily spread over one pixel.

Another approach to report Cassiopeia A on the map is to simulate how it could appear when observed by the same instrument used for the Sky continuum survey (see Fig. 5). For this purpose, the signal from Cassiopeia A is convolved with a Gaussian antenna beam with HPBW = 35′. One writes the T_b for the missing pixels (see F)

$$T_a = T_{Cont} + T_{HI}^* + T_{CMB} + \frac{T_{Cas\,A} G(\theta, \phi) \Omega_p}{\int_{4\pi} G(\theta, \phi) \sin\theta d\theta d\phi},$$ (5)

with $T_{Cont} + T_{CMB} \sim 3.12$ K.

---

[2]the location is ($\alpha = 350.30°; \delta = 58.54°$) in B1950 after conversion or equivalently ($\alpha = 23^h 21^m 10^s; \delta = 58°32'30”$) as reported by Rosenberg [9].
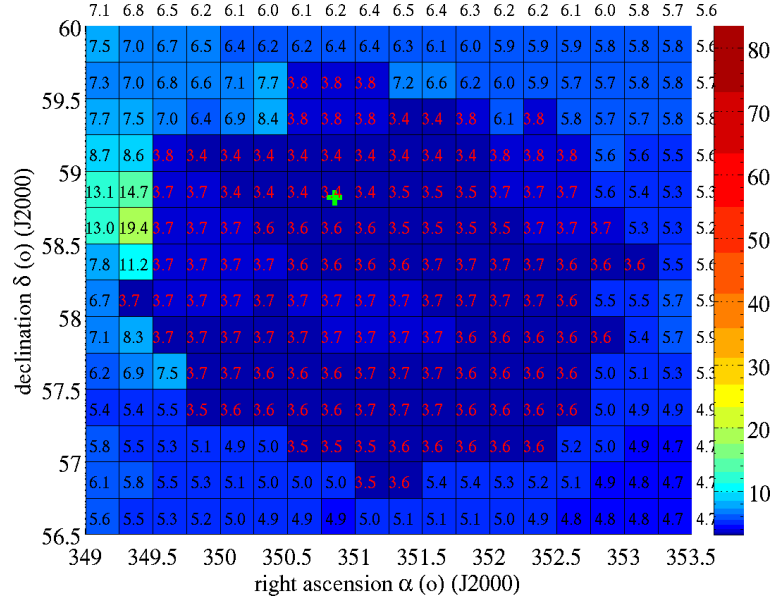
4

Figure 3: Location of Cassiopeia A in the sky (green +) reported in the J2000 equatorial coordinates system. The map is cropped around the area of interest. The numbers on the map report the Sky total T_b (K) rounded to the first decimal place for readability. They apply to the closest bottom-left node of the grid. The red numbers are for the missing pixels in the continuum survey (where $T_{\rm Cont} + T_{\rm CMB}$ is set to ~ 3.12 K, and the HI line contribution is the same as in Fig. 2), the black numbers are for data available in the survey.
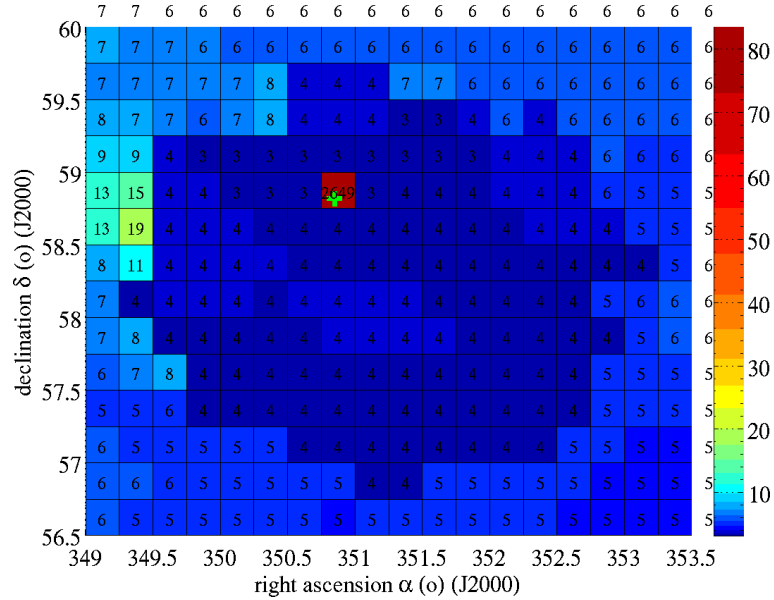

Figure 4: Map of sky brightness temperature (K) including the contribution for Cassiopeia A, assuming its flux spread over one pixel. Note that the Cassiopeia A pixel value (~ 2649 K) is out of the color scale bounds. The numbers on the map are rounded to closest integer for readability. They apply to the closest bottom-left node of the grid.

2.4 Total emission map

Figure 6 shows the total emission. It is the sum of the continuum, atomic hydrogen, cosmic background and Cassiopeia A component described previously (as per eq. (5)), all assumed unpolarized
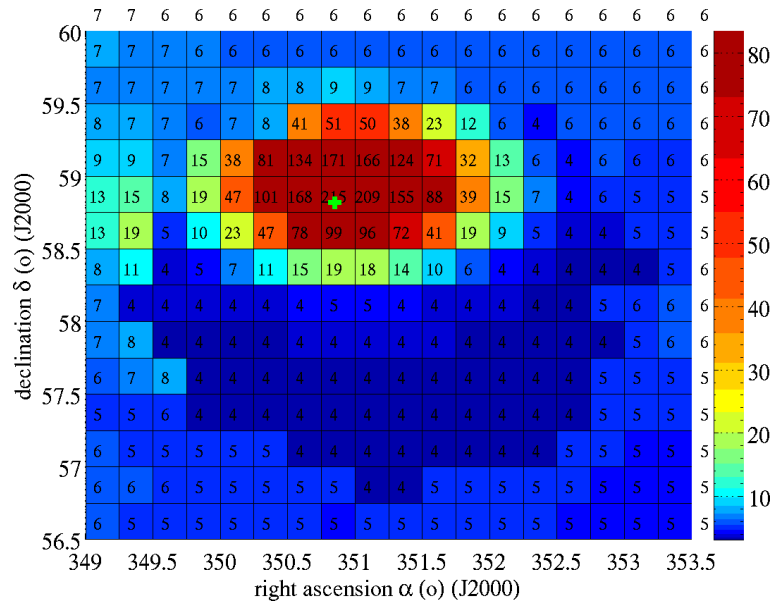
Figure 5: Map of sky brightness temperature (K) including the contribution for Cassiopeia A, assuming its flux convolved by the Stockert-like antenna beam. The numbers on the map are rounded to closest integer for readability.
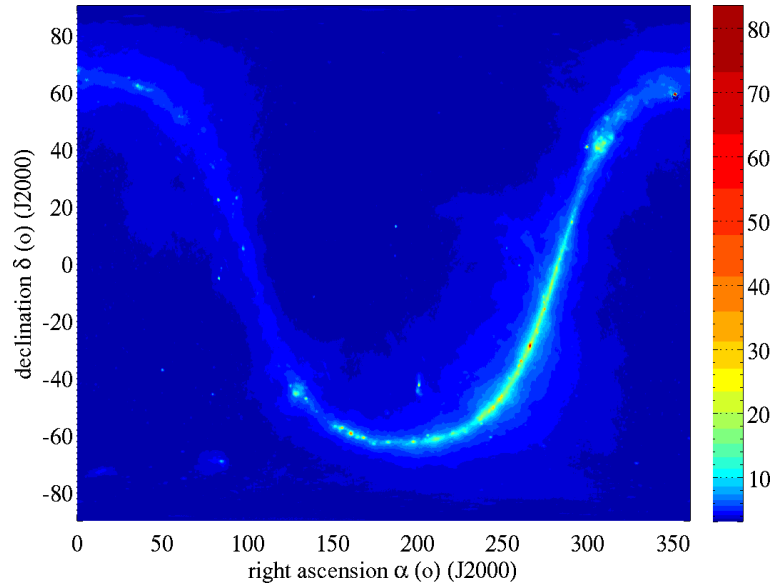

Figure 6: Total emission map of the sky, computed as the sum of the continuum, atomic hydrogen, cosmic background and Cassiopeia component (equivalent Stockert), all assumed unpolarized.

(see G). The map assumes a bandwidth $\Delta B_{\mathcal{A}} = 26$ MHz. The data are available as described in Section 1.2.

Acknowledgment

A Spectral index of continuum emission and Cassiopeia A at decimeter wavelengths

The dependence of the flux density S_ν of a source on frequency ν is characterized by the spectral index α_S such that

$$S_\nu \propto \nu^{\alpha_S} \tag{6}$$

In the literature, the spectral index refers also to the dependence of the T_b on ν. As $T_b \propto S_\nu \nu^{-2}$, the spectral index β_S for the T_b is defined by

$$T_b \propto \nu^{-\beta_S} \tag{7}$$

and is related to α_S by $\beta_S = 2 - \alpha_S$. Note that for blackbody radiation, $\beta_S = 0$ (the T_b is constant with the frequency) and $\alpha_S = 2$ (the flux density increases as the square of the frequency in the Rayleigh-Jeans domain).

For the sky continuum, α_S is in the range $[-0.9, -0.5]$ [11] or equivalently β_S is in the range $[2.5, 2.9]$. For Cassiopeia A, the spectral index varies in time. For the years 2010-2013, we use $\alpha_S = -0.727$ (see E).

B Impact of the difference between central frequencies of Sky surveys and radiometer center frequency

The sky survey data were acquired at a central frequency slightly different than the one at which Aquarius and other salinity remote sensing radiometers operate. In this section, the impact of this slight difference is quantified.

Define the relative difference between the galactic T_b at the frequency $\nu = 1420$ MHz and the one at a given frequency ν_m used for salinity measurement as

$$R_1 = [T_b(\nu_m) - T_b(1420)] / T_b(1420). \tag{8}$$

For a T_b spectral index β_S, the brightness temperature at a frequency ν (in MHz) can be written

$$T_b(\nu) = T_b(1420) \left(\frac{\nu}{1420}\right)^{-\beta_S} \tag{9}$$

and the relative difference simplifies to

$$R_1 = (\nu_m/1420)^{-\beta_S} - 1. \tag{10}$$

Results computed for the central frequency ($\nu_m = 1414$ MHz) at various spectral indices representative of the sky are reported in table 1. The relative difference between the T_b at the central frequencies of the survey and ν_m is of the order 1%.

β_S	2.4	2.7	3.0
$R_1(1414 \text{ MHz})$	+1.021%	+1.150%	+1.278%

Table 1: Relative difference between brightness temperatures at the frequency of 1420 MHz used for the continuum measurements and the frequency used for salinity measurements ν_m assuming various spectral indices β_S. Here $\nu_m = \nu_{\mathcal{A}} = 1414$ MHz (Aquarius).

C   Impact of changes in continuum Sky T_b inside the bandwidth of the radiometer

Typically, a radiometer integrates over a finite bandwidth. Over this bandwidth, the sky T_b is expected to vary slightly. This variation is quantified in this section following two approaches:

1. one quantifies the difference between the sky's T_b at the center of the band and at its bound, and

2. one quantifies the difference between the sky's T_b at the center of the band and the effective T_b derived from the flux integrated over the band.

For the first approach, similarly to (8), define the relative difference between the sky T_b at the central frequency ν_m where the measurements are performed and the one at a frequency bound ν_{lim} as

$$R_2 = \left[T_b(\nu_{\mathrm{lim}}) - T_b(\nu_m) \right] / T_b(\nu_m) \tag{11}$$

or, assuming a spectral index β_S,

$$R_2 = (\nu_{\mathrm{lim}}/\nu_m)^{-\beta_S} - 1. \tag{12}$$

Results computed for the band limits ($\nu_{\mathrm{lim}} = 1401$ MHz and $\nu_{\mathrm{lim}} = 1427$ MHz) are reported in table 2. The sky T_b at the bounds of the measurements frequency band differs from the one at the center of the band by a few percent.

β_S	2.4	2.7	3.0
$R_2(1401$ MHz$)$	+2.241%	+2.525%	+2.810%
$R_2(1427$ MHz$)$	-2.172%	-2.441%	-2.708%

Table 2: Relative difference between brightness temperatures at the frequency used for salinity measurements ν_m and the boundaries of the frequency band assuming various spectral indices β_S. Here $\nu_m = \nu_{\mathcal{A}}$ and the boundaries frequencies are 1401 MHz and 1427 MHz.

For the second approach, one defines the relative difference between the effective T_b over the radiometer bandwidth and the T_b at the center frequency. Define the effective brightness temperature T_{eff} as the temperature of a black body in thermal equilibrium which would radiate the same power over the band as the source does:

$$
\begin{aligned}
P &= 2k \int_{\nu_1}^{\nu_2} T_b(\nu)/\lambda^2 d\nu \\
&= 2k T_{\mathrm{eff}} \int_{\nu_1}^{\nu_2} 1/\lambda^2 d\nu
\end{aligned}
\tag{13}
$$

This leads to

$$T_{\mathrm{eff}} = \frac{\int_{\nu_1}^{\nu_2} T_b(\nu)/\lambda^2 d\nu}{\int_{\nu_1}^{\nu_2} 1/\lambda^2 d\nu}. \tag{14}$$

Replacing λ by $c \, / \, \nu$, one obtains

$$T_{\mathrm{eff}} = \frac{\int_{\nu_1}^{\nu_2} T_b(\nu)\nu^2 d\nu}{\int_{\nu_1}^{\nu_2} \nu^2 d\nu}. \tag{15}$$

Assuming a temperature spectral index of β_S, the brightness temperature at a frequency ν becomes

$$T_b(\nu) = T_b(\nu_m) \left(\frac{\nu}{\nu_m} \right)^{-\beta_S} \tag{16}$$

and the effective temperature becomes

$$T_{\text{eff}} = T_b(\nu_m) \frac{\int_{\nu_1}^{\nu_2} (\nu/\nu_m)^{-\beta_S} \nu^2 d\nu}{\int_{\nu_1}^{\nu_2} \nu^2 d\nu}$$
$$= T_b(\nu_m) \rho_{\text{eff}} \tag{17}$$

with

$$\rho_{\text{eff}} = \frac{1}{\nu_0} \frac{\int_{\nu_1}^{\nu_2} \nu^{2-\beta_S} d\nu}{\int_{\nu_1}^{\nu_2} \nu^2 d\nu}. \tag{18}$$

For $\beta_S \neq 3$,

$$\rho_{\text{eff}} = \frac{1}{\nu_0} \frac{\left[\frac{1}{3-\beta_S} \nu^{3-\beta_S} \right]_{\nu_1}^{\nu_2}}{[1/3\nu^3]_{\nu_1}^{\nu_2}} \tag{19}$$

and after rearranging, one finally obtains the ratio between the effective temperature and the T_b at $\nu_{\mathcal{A}}$ as

$$\rho_{\text{eff}} = \frac{1}{(1 - \beta_S/3)\,\nu_0^{-\beta_S}} \frac{\left(\nu_2^{3-\beta_S} - \nu_1^{3-\beta_S} \right)}{(\nu_2^3 - \nu_1^3)} \tag{20}$$

For $\beta_S = 3$,

$$\rho_{\text{eff}} = \frac{3}{\nu_0^{-3}} \frac{(\ln \nu_2 - \ln \nu_1)}{(\nu_2^3 - \nu_1^3)} \tag{21}$$

Then, one defines the relative difference in T_b as

$$R_3 = \frac{[T_{\text{eff}} - T_b(\nu_m)]}{T_b(\nu_m)}$$
$$= \rho_{\text{eff}} - 1. \tag{22}$$

The results for the radiometer in this example are reported in table 3 and show a very small difference between the sky T_b at the central frequency and the effective T_b associated with the brightness over the whole measuring band.

β_S	2.4	2.7	3.0
R_3	-2.10^{-3} %	-1.10^{-3} %	$+1.10^{-7}$ %

Table 3: relative differences between effective brightness temperatures integrated over the Aquarius frequency band $B_{\mathcal{A}} = [1401 - 1427]$ MHz with various spectral indices β_S and the brightness temperature at the Aquarius central frequency $\nu_{\mathcal{A}} = 1414$ MHz.

D Derivation of an effective brightness temperature in a small bandwidth

The brightness B over a bandwidth $\Delta\nu = (\nu_0 + \Delta\nu \,/\, 2) - (\nu_0 - \Delta\nu \,/\, 2) = \nu_2 - \nu_1$ is derived integrating the spectral brightness, function of $T_b(\nu)$, according to

$$B = \int_{\nu_1}^{\nu_2} 2k/\lambda^2 T_b(\nu) d\nu. \tag{23}$$

Define the effective brightness temperature T_b^* so that a source with the brightness temperature T_b^* constant over $\Delta\nu$ would have the brightness B in (23). Therefore, one wants

$$
\begin{aligned}
B^* &= \int_{\nu_1}^{\nu_2} 2k/\lambda^2 T_b^* d\nu, \\
&= B
\end{aligned}
\tag{24}
$$

Extracting T_b^* from the integral in (24) and using (23) for B, one derives

$$
\begin{aligned}
T_b^* &= \frac{\int_{\nu_1}^{\nu_2} 2k/\lambda^2 T_b(\nu) d\nu}{\int_{\nu_1}^{\nu_2} 2k/\lambda^2 d\nu}, \\
&= \frac{\int_{\nu_1}^{\nu_2} T_b(\nu)/\lambda^2 d\nu}{\int_{\nu_1}^{\nu_2} 1/\lambda^2 d\nu}.
\end{aligned}
\tag{25}
$$

If one assumes $1/\lambda^2$ varying little over $\Delta\nu$ (with $\Delta\nu = 2\,\mathrm{MHz}$ and $\nu_0 = 1420\,\mathrm{MHz}$, $1/\lambda^2$ varies by $\sim 0.3\%$) so that it can be extracted from the integrals in (25), one derives the simple expression

$$
T_b^* = \frac{1}{\Delta\nu} \int_{\nu_1}^{\nu_2} T_b(\nu) d\nu.
\tag{26}
$$

E   Flux density of Cassiopeia A at 1.4 GHz for the period 2010-2013
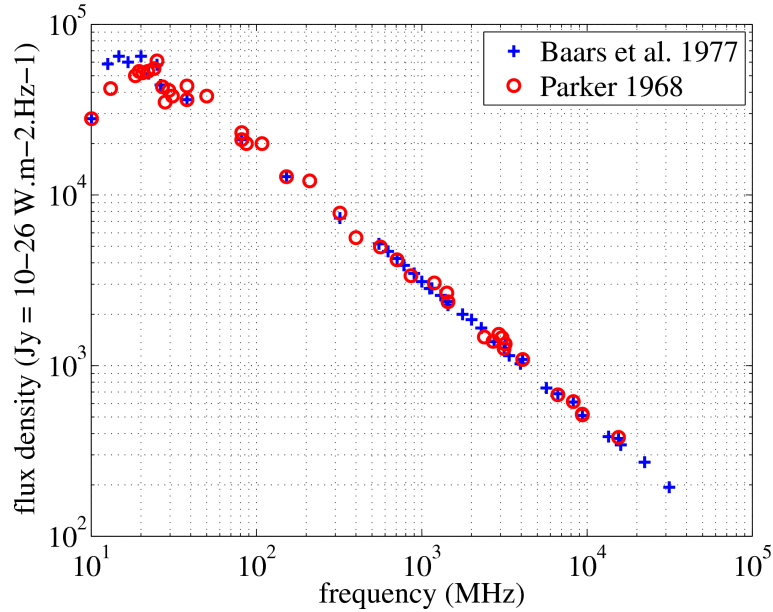

Figure 7:   Flux density of Cassiopeia A measured between years 1955 and 1973 and between frequencies 10 MHz and 31 GHz.

Cassiopeia A flux density varies with frequency and time [12, 13]. Therefore, to derive the flux density relevant to Aquarius, one must transform existing measurement to the proper frequency (1.414 GHz) and time (2010 - 2013). Parker reports historical measurements performed between the years 1955 and 1967 and the frequencies 10 MHz and 15.5 GHz. He adopts a temporal decrease for the flux density of 1.1±0.18% per year [12]. Baars et al. [13] report measurements performed
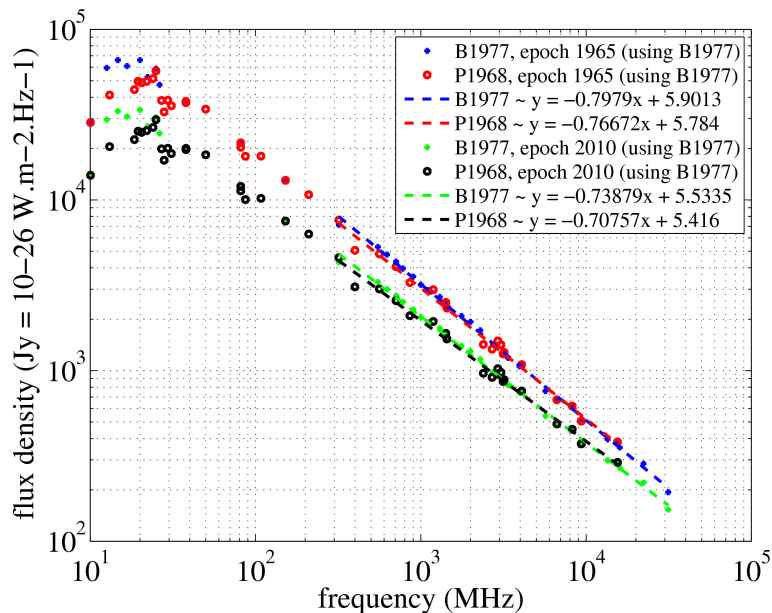
Figure 8: Same as Fig. 7 with measurements expressed in epoch 1965 and 2010, and with linear regression fit for frequencies larger than 300 MHz (see legend for results of fits).

between 1959 and 1973 and 10.05 MHz and 31.41 GHz. They propose the following law for the decrease in flux density

$$dS/S = 0.0097 - 0.0030 \log_{10} \nu \qquad (27)$$

where the frequency ν is in GHz and dS/S is the relative decrease in flux density per year (note: $\log_{10}$ is the base 10 logarithm). At a frequency $\nu = 1.414$ GHz, the decrease is about 0.92% per year, a value relatively close to the one chosen by Parker.

The raw data reported by Parker and Baars et al. is presented in Fig. 7. Both data sets are in relatively good agreement, particularly in the high frequency domain. These data are also expressed at the epochs 1965 and 2010 (that is our epoch of interest) in Fig. 8 using (27). The transformation to epoch 1965 leads small changes only, but the transformation to 2010 induces a significant decrease of flux density at all frequencies and a noticeable change of spectral shape. We derive linear regressions of the spectral data for frequencies larger than 300 MHz using both data sets separately (see legend in Fig. 8 for results). Both regressions lead to similar results, the flux density at 1.414 GHz derived from both data sets differing by less than 5%. In order to use all data available, we use a linear regression on the merged data sets for the year 2010. We find the following spectral function

$$\log_{10} S_{\mathrm{CasA}}(\nu) = -0.7269 \log_{10} \nu + 5.4882 \qquad (28)$$

with ν the frequency in MHz and S_{CasA} the flux density in Jansky ($\log_{10}$ is the base 10 logarithm). The flux density calculated at 1414 MHz for 2010 is $S_{\mathrm{CasA}}(1414) = 1578$ Jy. Extrapolating for the year 2013 using (27) leads to $S_{\mathrm{CasA}}(1414) = 1534$ Jy. For the final map, we use an approximated value of 1600 Jy, leading to an error of less than 5% for the period 2010-2013.

F   Convolution of Cassiopeia A by a Stockert-like antenna beam

The brightness temperature (T_b^m) measured in the direction (θ, ϕ) by an antenna with a gain pattern G is

$$T_b^m(\theta, \phi) = \frac{\int_{4\pi} T_b^S(\theta', \phi') G(\theta', \phi')\, d\Omega'}{\int_{4\pi} G(\theta', \phi') d\Omega'} \tag{29}$$

with T_b^S the brightness temperature of the Sky. The upper integral can be parted as

$$T_b^m = \frac{\int_{\mathrm{CasA}} T_b^{\mathrm{CasA}}(\theta', \phi') G(\theta', \phi')\, d\Omega'}{\int_{4\pi} G(\theta', \phi') d\Omega'} + \frac{\int_{4\pi \setminus \mathrm{CasA}} T_b^S(\theta', \phi') G(\theta', \phi')\, d\Omega'}{\int_{4\pi} G(\theta', \phi') d\Omega'}, \tag{30}$$

with the first integral performed over Cassiopeia A and the second integral over the remaining portion of the Sky. One sets the second integral to zero: it is not clear how much the pixels surrounding the missing pixels already account for Cassiopeia A contribution, and they are already smoothed by the antenna pattern. In addition, the contribution in (30) is to be added to the background map in Fig. 3, therefore a background contribution of about 3.4 K is already included. One obtains

$$T_b^m = \frac{\int_{\mathrm{CasA}} T_b^{\mathrm{CasA}}(\theta', \phi') G(\theta', \phi')\, d\Omega'}{\int_{4\pi} G(\theta', \phi') d\Omega'}. \tag{31}$$

The previous expression can be approximated by

$$T_b^m = \frac{T_b^{\mathrm{CasA}\,*} G(\theta_{\mathrm{CasA}}, \phi_{\mathrm{CasA}}) \Omega_{\mathrm{CasA}}}{\int_{4\pi} G(\theta', \phi') d\Omega'} \tag{32}$$

if one neglects the variation of the gain over Cassiopeia A extent, and assumes the brightness temperature of Cassiopeia A to be constant and equal to $T_b^{\mathrm{CasA}\,*}$. The latter assumption is not required if one states that

$$T_b^{\mathrm{CasA}\,*} = \frac{1}{\Omega_{\mathrm{CasA}}} \int_{\mathrm{CasA}} T_b^{\mathrm{CasA}}(\theta', \phi')\, d\Omega' \tag{33}$$

or simply use an effective $T_b^{\mathrm{CasA}\,*}$ derived from the flux density as in (4).

Here we assume an antenna with a Gaussian beam and a HPBW = 35 arcmins ~ 0.58 degrees, with

$$G(\theta_A) = \frac{1}{N} \exp\left[-0.5\left(\frac{\theta_A}{\theta_0}\right)^2\right] \tag{34}$$

where θ_A is the angle off boresight, $\theta_0 \sim 0.2463$ degrees so that $G(\mathrm{HPBW}/2) = 0.5$ and the normalization is computed as $N = \int_{4\pi} G(\theta', \phi') d\Omega' = 1.1612 \times 10^{-4}$.

In order to compute the convolved Cassiopeia A temperature for a pixel in a direction (θ, ϕ) using (32), one must compute the gain in the direction of Cassiopeia A. One first computes θ_A as the angular distance between the given pixel and the source Cassiopeia A (see Fig. 9). Then one derives the antenna gain (see Fig. 10) and the temperature as it would be measured by the Gaussian beam antenna (see Fig. 11). It should be noted that integrating the resulting effective convolved Cassiopeia A T_b (reported in Fig. 11) according to

$$S^*(Jy) = 2k/(\lambda^2 \times 10^{-26}) \int T_b^m(K) \sin\theta d\theta d\phi \tag{35}$$

leads to a flux density $S^* = 1568$ Jy, slightly different of the assumed flux of 1600 Jy only because the spread was limited to the missing pixels instead of applied to the whole map.

G   Polarization of the Sky background

The background map (Fig. 6) presented here assumes that the signal is unpolarized. Data on the degree of polarization at L-band has recently been published. The large-scale polarization of the Sky background was measured in the vicinity of ν_0 by Wolleben et al. [14] for the Northern sky and Testori et al. [15] for the Southern sky. The first survey was conducted at a central frequency
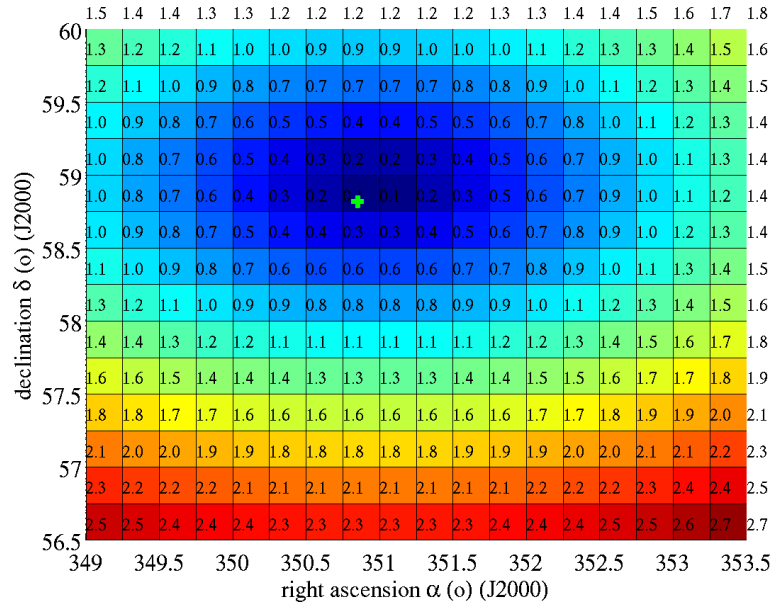
Figure 9: Map of the angular distance (degrees) between pixels and Cassiopeia A. The numbers on the map are rounded to the first decimal place for readability.
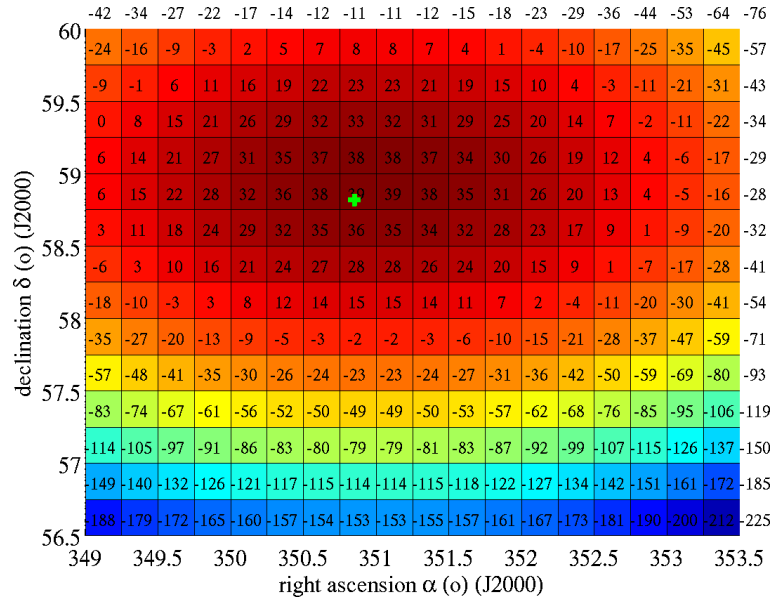

Figure 10: Map of the Gaussian beam gain (dB) in the direction of Cassiopeia A when pointing at the various pixels on the map. The numbers on the map are rounded to closest integer for readability.

of 1410 MHz with a bandwidth of 12 MHz (10 Mhz for some of the measurements). That sets the upper bound of the frequency band at 1416 MHz, less than the lower bound of the HI emission band. The latter survey was conducted at a central frequency of 1435 MHz, with a bandwidth of 14 MHz, avoiding the HI band too. Claimed accuracies are ∼15 mK r.m.s. noise, less than 50 mK systematic error and a pointing accuracy of the order of the arc minute.
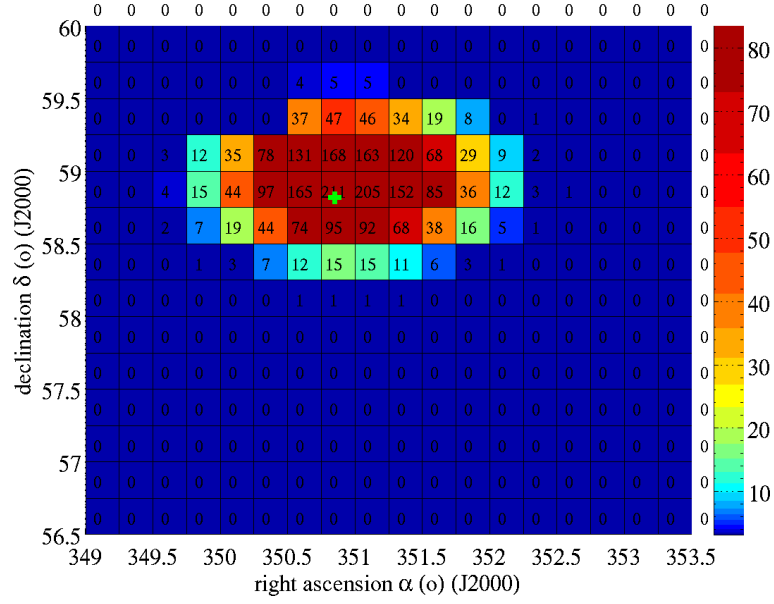
Figure 11: Map of effective Cassiopeia A brightness temperature (K) after convolution by the Stockert-like antenna beam (only so-called missing pixel are modified). The numbers on the map are rounded to closest integer for readability.

G.1 Merging the data sets for northern and southern sky.

Maps for polarization are available for the northern (DRAO, [14]) and southern sky seperatly (Villa Elisa, [15]), but no merged product exists to our knowledge. The goal of this section is to describe the method used to merge the two maps into one, and to perform some basic sanity check on the data. Both maps were downloaded at the address `http://www.mpifr-bonn.mpg.de/survey.html` in J2000 RA/DEC coordinates at the original resolution (i.e. $0.25°$). The map from both survey are reported in Fig. 12. They overlap each other for declinations between -10° and -29°.

The differences between the two map over the overlapping region are reported in Fig. 13. A scatterplot of the data from both survey is reported in Fig. 14.

In order to merge the surveys, the data over the overlapping region are averaged between the two maps.

G.2 Analysis of the polarization of the Sky background

Figure 15 reports the map of the polarized Sky. The general structure of the map is very different from the emission maps in figures 1 and 2. The Galactic plane does not exhibit a particularly large polarization, and the map is characterized by large structures with a dynamic range of the order of 2K.

Figure 16 reports the histogram for the polarized maps in figure 15. The polarization translates in third and fourth Stokes mostly between $-0.5K$ and $+0.5K$, with maxima up to ±2 K. The polarized emission is ignored in the final map.

3rd Stokes, northern sky

4th Stokes, northern sky

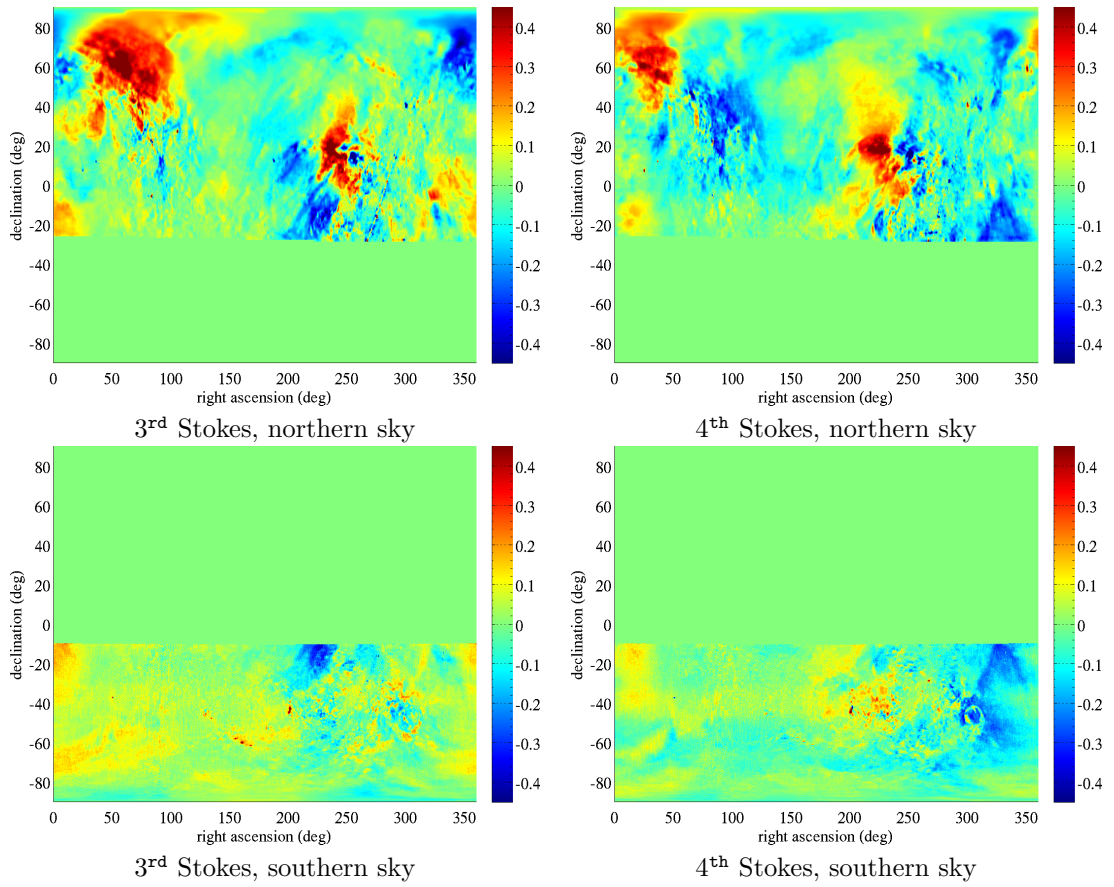3rd Stokes, southern sky

4th Stokes, southern sky

Figure 12: Map of (left column) the third Stokes parameter and (right column) the forth Stokes parameter, from (top row) the northern sky survey and (bottom row) the southern sky survey. The colorscale is arbitrarily saturated.
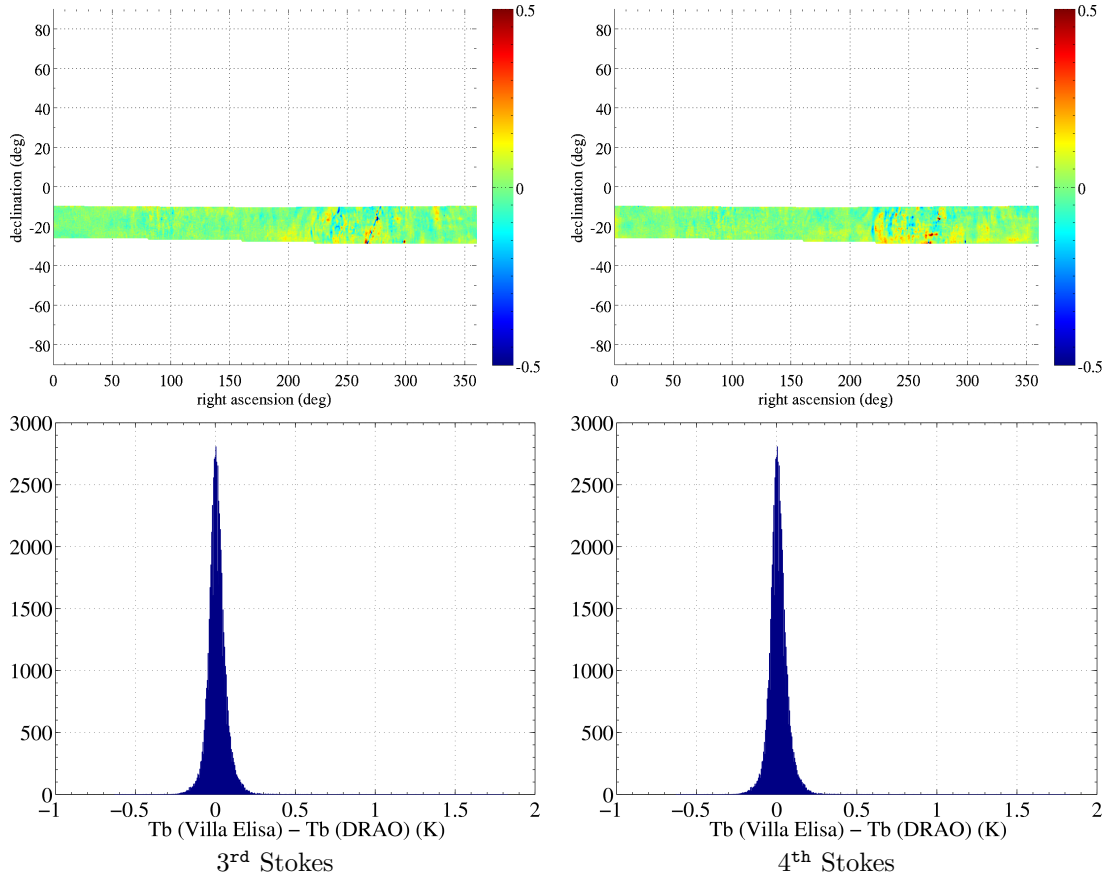
Figure 13: (top row) Map and (bottom row) histogram of the differences between the southern sky map and the northern sky maps (see Fig. 12) over the overlapping region.
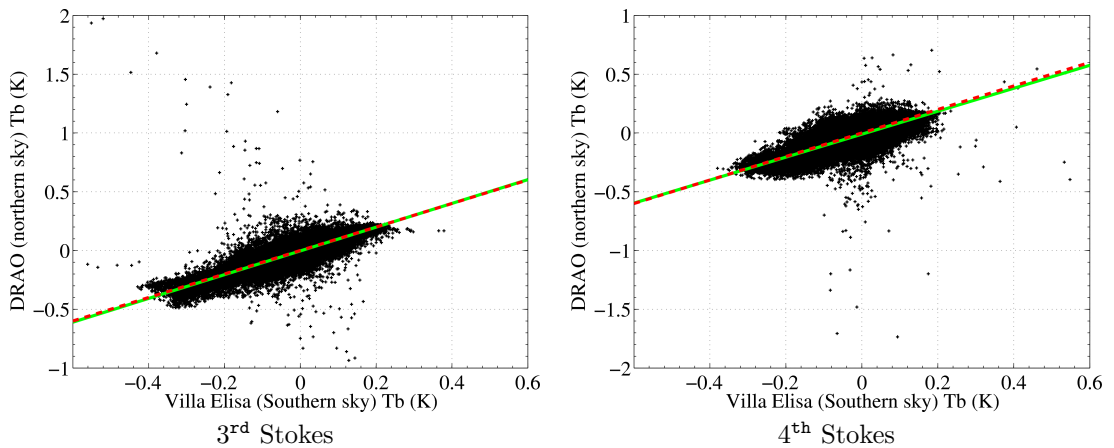
Figure 14: Scatterplot of the data from the northern and southern sky survey. The green line represent a linear regression through the data and the red dashed line has a slope of 1. The correlation coefficients are 0.83918 and 0.8272 for the third and forth Stokes parameters respectively.
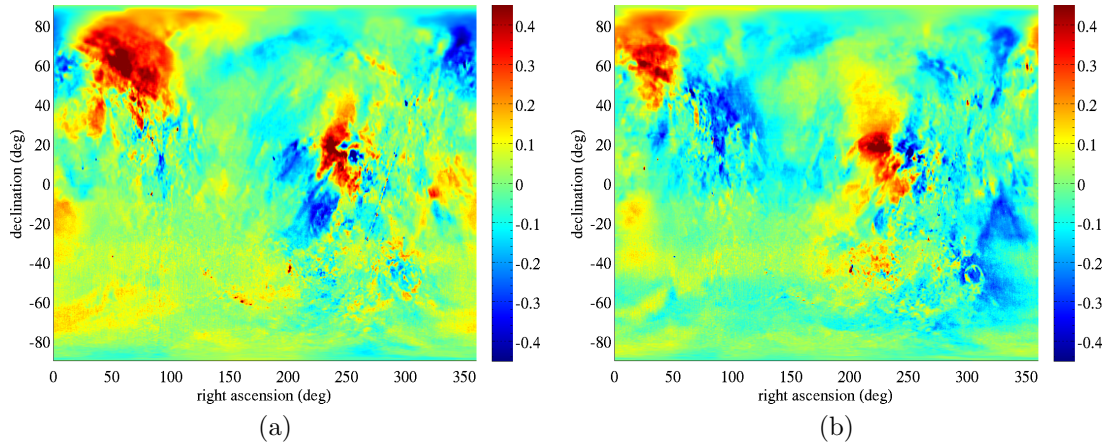
Figure 15: Maps of (a) the third Stokes parameter in K and (b) the fourth Stokes parameter in K [14, 15]. The colorscale has been arbitrarily bounded at ±0.45 K.
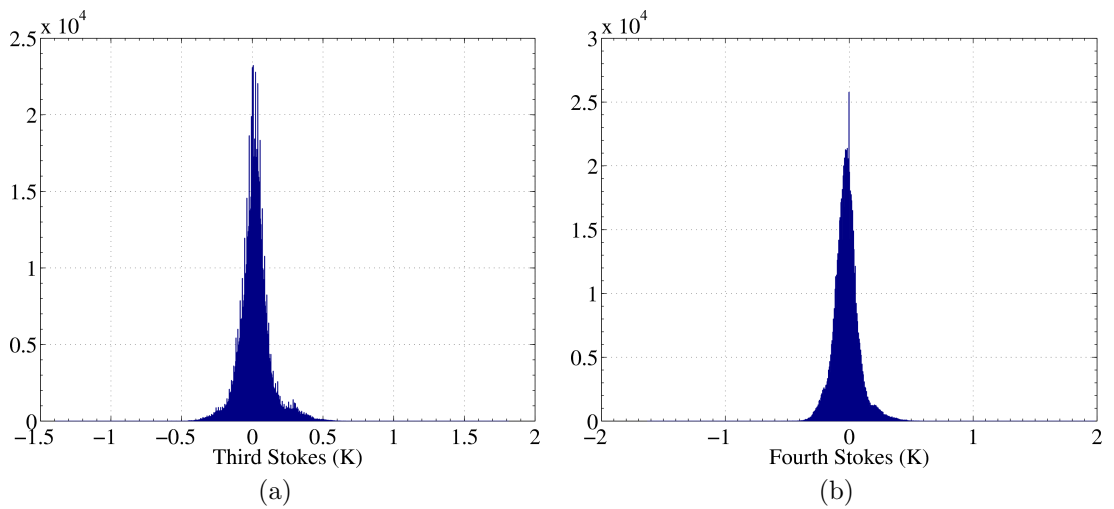

Figure 16: Histograms of (a) the third Stokes parameter and (b) the fourth Stokes parameter.

H Document history

August 2010: Section 2.3 and E have been rewritten. The solid angle of the pixel at Cassiopeia A location (see (4) and text below it) now writes $\Omega_p = \cos\delta(0.25°)^2 \simeq 9.8572 \times 10^{-6}$ sr instead of $\Omega_p = \sin\delta(0.25°)^2 \simeq 1.629 \times 10^{-5}$ sr. We would like to thank Franck Wentz for reporting the error to us. Data files have been updated accordingly.

   May 2018: Section 1.2 has been modified to reflect the new format for the datafile and the new location of the data now at NASA PO.DAAC.

I Glossary

References

[1] D. M. Le Vine, G. S. E. Lagerloef, F. R. Colomb, S. H. Yueh, and F. A. Pellerano, "Aquarius: An instrument to monitor sea surface salinity from space," vol. 45, no. 7, pp. 2040–2050, July 2007.

[2] W. Reich, "A radio continuum survey of the northern sky at 1420 mhz. Part I," *Astronomy and Astrophysics Supplement Series*, vol. 48, pp. 219–297, May 1982.

[3] P. Reich and W. Reich, "A radio continuum survey of the northern sky at 1420 MHz. Part II," *Astron. Astroph. Suppl. Ser.*, vol. 63, pp. 205–292, 1986.

[4] J. C. Testori, P. Reich, J. A. Bava, F. R. Colomb, E. E. Hurrel, J. J. Larrarte, W. Reich, and A. J. Sanz, "A radio continuum survey of the southern sky at 1420 MHz observations and data reduction," *Astronomy & Astrophysics*, vol. 368, pp. 1123–1132, 2001.

[5] P. Reich, J. C. Testori, and W. Reich, "A radio continuum survey of the southern sky at 1420 MHz the atlas of contour maps," *Astronomy & Astrophysics*, vol. 376, pp. 861–877, 2001.

[6] D. Hartmann and W. B. Burton, *Atlas of Galactic Neutral Hydrogen*. Cambridge University Press, 1997.

[7] E. M. Arnal, E. Bajaja, J. J. Larrarte, R. Morras, and W. G. L. Poppel, "A high sensitivity HI survey of the sky at $\delta \leq -25°$," *Astronomy and Astrophysics Supplement*, vol. 142, pp. 35–40, 2000.

[8] P. M. W. Kalberla, W. B. Burton, D. Hartmann, E. M. Arnal, E. Bajaja, R. Morras, and W. G. L. Poppel, "The Leiden/Argentine/Bonn (LAB) survey of galactic HI. Final data release of the combined LDS and IAR surveys with improved stray-radiation corrections," *Astronomy and Astrophysics*, vol. 440, no. 2, pp. 775–782, September 2005.

[9] I. Rosenberg, "Distribution of brightness and polarization in Cassiopeia A at 5.0 GHz," *Monthly Notices of the Royal Astronomical Society*, vol. 151, pp. 109–122, 1970.

[10] B. S. Mason, E. M. Leitch, S. T. Myers, J. K. Cartwright, and A. C. S. Readhead, "An absolute flux density measurement of the supernova remnant Cassiopeia A at 32 GHz," *The Astronomical Journal*, vol. 118, pp. 2908–2918, August 1999.

[11] P. Reich and W. Reich, "A map of spectral indices of the Galactic radio continuum emission between 408 MHz and 1420 MHz for the entire northern sky," *Astronomy & Astrophysics Supplement Series*, vol. 74, no. 1, pp. 7–23, July 1988.

[12] E. Parker, "Precise measurements of the flux densities of the radio sources Cas A and CygG A at metre wavelengths," *Mon. Notic. Roy. Astron. Soc.*, vol. 138, pp. 407–422, 1968.

[13] J. W. M. Baars, R. Genzel, I. I. K. Pauliny-Toth, and A. Witzel, "The absolute spectrum of CAS A - an accurate flux density scale and a set of secondary calibrators," *Astronomy and Astrophysics*, vol. 61, no. 1, pp. 99–106, October 1977.

[14] M. Wolleben, T. L. Landecker, W. Reich, and R. Wielebinski, "An absolutely calibrated survey of polarized emission from the northern sky at 1.4 GHz observations and data reduction," *Astronomy & Astrophysics*, vol. 448, pp. 411–424, 2006.

[15] J. C. Testori, P. Reich, and W. Reich, "A fully sampled λ21 cm linear polarization survey of the southern sky," *Astronomy & Astrophysics*, vol. 484, pp. 733–742, 2008.